Eurographics Workshop on Visual Computing for Biology and Medicine (2026)
R. Krueger, E. Mörth and K. Furmanová (Editors)

Conference Paper

BeLOVE X-Talker: Interactive Heart-Brain Cross-Talk Explorer

M. Huellebrand[1,2,3,4], A. P. Laube[1,2,3], H. F. Ali[2,5,6], J. E. Weber[2,3,5,7,8], I. Rohrpasser-Napierkowski[7], J. Schulz-Menger[2,3,9,10], K. Villringer[2,5] and A. Hennemuth[1,2,3,4] on behalf of the BeLOVE Study Group

[1]Deutsches Herzzentrum der Charité, Institute of Computer-assisted Cardiovascular Medicine, Berlin, Germany.
[2]Charité – Universitätsmedizin Berlin, corporate member of Freie Universität Berlin and Humboldt Universität zu Berlin, Germany.
[3]DZHK (German Centre for Cardiovascular Research), partner site Berlin, Berlin, Germany
[4]Fraunhofer Institute for Digital Medicine MEVIS, Bremen, Germany
[5]Center for Stroke Research Berlin (CSB), Charité – Universitätsmedizin Berlin, Germany
[6]Einstein Center for Neurosciences, Charité – Universitätsmedizin Berlin, Germany
[7]Berlin Institute of Health (BIH) at Charité – Universitätsmedizin Berlin, Germany
[8]Department of Neurology and Experimental Neurology, Charité–Universitätsmedizin Berlin
[9]Experimental and Clinical Research Center, a joint cooperation between Charité and MDC, Cardiology and WG on CMR Berlin, Germany
[10]Department of Cardiology and Nephrology, HELIOS Klinikum Berlin Buch, Germany

Abstract

The interaction between brain and heart in disease processes is subject to many ongoing studies. In order to enable the analysis of correspondences and differences in tissue properties of brain and heart muscle, we developed a processing pipeline for the automatic extraction of tissue biomarkers from MRI relaxometry using anatomical atlases. For the interactive exploration, we combined a parallel coordinate plot with geometric representations of these atlases. In two use cases, we compared surface visualizations with color and transparency to glyph representations in the geometrical context of the atlases. User feedback indicated the usefulness for the detection of differences and correspondences between regions in brain and heart.

CCS Concepts

• ***Human-centered computing*** → *Visual analytics; Visualization systems and tools;* • ***Computing methodologies*** → *Image processing;*

1. Introduction

The analysis of medical imaging data frequently requires the simultaneous consideration of multiple interdependent variables, ranging from numerical biomarkers and demographic metadata to their spatial relations to anatomical structures. The effective visual analysis of such multivariate, multimodal data demands coupled representations that integrate abstract, attribute-oriented views with their spatial context [KH13]. In cohort studies that include imaging data from multiple organs, heterogeneity in data acquisition, imaging protocols and scanner sites add to the complexity and demand data processing approaches that allow a joint analysis across subjects. Established strategies include linked-view interfaces that juxtapose statistical summaries over cohorts with anatomical renderings [SMB*10, AOH*14].

Recent clinical research has increasingly focused on systemic interactions between the heart and brain. The two organs communicate bidirectionally via autonomic, neurohormonal, and vascular pathways to maintain cardiovascular homeostasis and cerebral perfusion, and an impairment of this cross-talk can lead to cardiac injury following neurological disease and vice versa [SVM*26, GTYS25]. Understanding these mechanisms is clinically relevant for cardio-cerebrovascular diseases, yet it requires the joint comparison of complementary tissue properties across two spatially separate organs. Advanced MRI provides such complementary quantitative biomarkers: cardiac T1 and T2 mapping is sensitive to diffuse myocardial fibrosis, edema, and inflammation, while parametric brain mapping (R1, R2*) characterizes structural and functional tissue alterations. Investigating the heart–brain axis therefore inherently demands a multivariate analytical approach that compares these parameters across distinct anatomical regions in two organs, while accounting for population-level covariates. In multi-center cohort studies such as the Berlin Longterm Observation of Vascular Events (BeLOVE) [WAB*23] this complexity is compounded through the image acquisition across multiple scanners and vendors, as well as initial patient diagnoses, yielding heterogeneous, high-dimensional datasets that span multiple organs, parameters, and subjects.

From the requirements of heart–brain cross-talk analysis in a

DOI: 10.2312/vcbm.20261009

multi-center cohort, we derive four analytical goals that guide our design:

- G1 – Spatially resolved display: Jointly display regional parameters (T1, T2, R1, R2*) in corresponding heart and brain regions within one shared frame.
- G2 – Subgroup filtering: Interactively select patient subgroups by demographic, diagnostic, and biomarker variables.
- G3 – Detection of differences: Reveal local differences and co-occurring patterns between subgroups, within one organ and across the heart–brain axis.
- G4 – Intra-group variability: Communicate not only mean values but also their variability, so differences can be judged against subgroup heterogeneity.

To address these goals, we present BeLOVE X-Talker, a processing and visual exploration approach designed for this multivariate, multi-organ cohort analysis problem. Following the linked-view paradigm for multivariate spatial data [KH13], our framework integrates a processing pipeline standardizing quantitative maps and extracting tissue biomarkers using standard anatomical atlases (G1), with an interactive front-end in which a single parallel coordinate plot (PCP) — serving as an abstract, high-dimensional filter (G2) — simultaneously controls two anatomically standardized atlas spaces, the cardiac AHA model and the cerebral arterial-territory atlas. Because a subgroup defined once in the parallel coordinate plot is propagated identically to both organ views, every regional cardiac and cerebral statistic is, by construction, computed over the same patient subgroup. This coordinated cross-atlas filtering is what turns two independent organ views into a single instrument for cross-organ hypothesis generation (G1, G3). Within this frame we compare two spatial encodings: glyph-based representations, which compactly encode statistical moments through parametric geometry and color, and surface-based representations, which directly map mean values and variability onto anatomical structures via color and transparency (G3, G4). We demonstrate the utility of the integrated approach through two use cases involving subgroup comparisons based on clinical diagnosis and obesity metrics.

2. Related Work

2.1. Comparability of Multi-Organ Imaging Data

Analyzing cardiac (T1, T2) and cerebral (R1, R2*) relaxometry parameters jointly across a cohort requires that the underlying data be comparable, both between subjects and across organs. Variability in imaging data from study cohorts is often introduced through heterogeneous data origin (different sites, imaging protocols, scanner vendors) and harmonization approaches exist to mitigate these batch effects, either on a feature or image level [YSZG26]. Most recently, generative learning approaches have been utilized for harmonization [ZDL*21, ZLX*23, BLA*25, LSW*26].

Imaging studies often employ registration to a common anatomical model to achieve comparability between patients. In the context of the brain, non-rigid registration to a template brain (e.g. the Montreal Neurological Institute (MNI) template) [MMD12] leads to a common coordinate system, but may also alter spatial intensity distributions within the image producing undesirable feature distortions. Alternatively, structural models called atlases may be fitted to the images, and thus facilitate the identification of common substructures across patients without image deformation.

The choice of atlas or model depends on the desired granularity and functional regions that are analyzed. For the heart, the American Heart Association 17-segment model of the left myocardium uses anatomical landmarks to divide the left ventricle into segments that correlate loosely with coronary artery distribution, hence facilitating standardized reporting of the location of findings [CWD*02]. For the brain, a multitude of atlases exist that delineate functional or structural regions (see https://www.humanbrainproject.eu/en/science-development/focus-areas/brain-atlases/ for examples). Analogously to the AHA model, the cerebral artery territory atlas [LHX*23] maps regions belonging to one of the major blood vessels supplying the brain, and is used in this work.

2.2. Glyph Representation

Glyphs serve to visualize multi-variate data [ROP11] and are employed to illustrate high-dimensional parameters in both cardiovascular [CNS*15] and neurological [BSJ*14] contexts. Encoding quantitative parameters through placement, orientation, size, shape and color allows the simultaneous visual analysis of relationships that may otherwise be elusive.

2.3. Cohort Visualization and Exploration Tools

Several interactive tools exist for the visual and quantitative analysis of imaging data. ParaGlyder [MHBS20] employs different visualization techniques to aggregate and represent the underlying data, including star-shaped glyphs ("stixels") and linked views to additional plots, but supports the exploration of a single patient. For multimodal cohort data that include image data, most authors [AOH*14, MNB*23, HIT*22] adopt linked visualizations that couple interactive plots with anatomy-related renderings, following Steenwijk et al. [SMB*10]. VisualNeuro [JBF*20] takes a similar approach, displaying multivariate clinical parameters on a parallel coordinate plot and image-derived parameters on an anatomical model to highlight spatial correlations. Cohort visualization systems from other domains employ closely related visual idioms: Wentzel et al. [WHL*20] combine dot-glyphs with transparent anatomical outlines to explore and predict outcomes across a radiation-therapy cohort.

However, these approaches operate within a single anatomical system. In the specific context of the heart–brain axis, region-based analysis using standardized atlases has so far been applied only to summarize correspondences with Sankey diagrams [MBPA*25], and, as in most cohort visualizations [GRF*24, XCL*25], the associated interactive tool (available at https://www.cbica.upenn.edu/bridgeport) still provides anatomy-related visualizations of the brain alone. To our knowledge, no existing approach couples two anatomically unrelated organ atlases within one linked frame.

Extending cohort exploration from one anatomy to two is not merely a matter of adding a second viewport: it requires that subgroup definition be shared across organs so that any observed cross-organ pattern is attributable to the cohort rather than to divergent

selections. We therefore design the interface around synchronized heart–brain views driven by a single coordinated filter, so that users can compare parameter distributions not only within an organ but also across organs and disease-defined subgroups. Our glyph-plus-transparent-surface encoding is conceptually related to Wentzel et al. [WHL*20], but we apply it to the joint analysis of two anatomically distinct organs, each standardized onto its respective atlas, within one linked frame — a multi-organ setting not addressed by prior cohort tools.

3. Materials and Methods

3.1. Data

The BeLOVE study [WAB*23] (Berlin Longterm Observation of Vascular Events; https://drks.de/search/de/trial/DRKS00016852) includes patients with recent acute cardiovascular events (acute heart failure, acute coronary syndrome, acute stroke, transient ischaemic attack or non-traumatic intracerebral hemorrhage), as well as patients at high cardiovascular risk, but without event in the past year. Participants receive comprehensive imaging assessment approximately 90 days after index event, at one of three clinical research units. The study protocol was approved by the Ethics Committee of Charité–Universitätsmedizin Berlin (EA1/066/17), and all BeLOVE participants provided written informed consent.

Magnetic resonance imaging data is collected of both the heart and the brain on either Siemens or Philips scanners, including quantitative mapping (T1, T2, and multi-parametric mapping R1, R2*, respectively). At the time of analysis, 528 patient datasets were available for our investigation, see Table 1.

	n = 528
Male	372 (70%)
Age, years	62.8 ± 11.9
BMI, kg/m^2	28.5 ± 5.3
Waist-to-Hip Ratio	0.98 ± 0.09
LV Ejection Fraction, %	59 ± 9
Initial Diagnosis	
Stroke	264 (50%)
Acute Coronary Syndrome	119 (23%)
Diabetes	128 (24%)
Acute Kidney Failure	8 (1%)
Heart Failure	9 (2%)

Table 1: *BeLOVE patient characteristics*

3.2. Image Processing

Anatomical regions of interest (ROI) were defined in the cardiac and neuro images using nnU-Net based segmentation models [IJK*21]. In the heart, the left ventricle was delineated in the three slices of the short-axis scans. In the brain, gray and white matter were segmented, excluding subcortical structures. The segmentation model for the brain has been trained on MPRAGE images of the public OASIS dataset [MWP*07], and segmentation labels of the quantitative R1 and R2* maps were obtained by registering the corresponding MPRAGE image to the maps. Example images and their segmentations can be seen in Figure 1.

To obtain spatially resolved feature distributions, the myocardial ROI was subdivided into segments according to the 17-segment AHA model [CWD*02], and the brain according to the arterial territory atlas [LHX*23], see Figure 2. The results are patient-specific anatomical region label masks.

We extract mean values and standard deviation per region for T1, T2, R1 and R2*.

3.3. Visualization

The design follows the linked-view paradigm for multivariate spatial data [KH13], separating the abstract attribute space (PCP, addressing G2) from the spatial context (3D atlases, addressing G1). To investigate the spatial distribution of mean T1, T2, R1, and R2* values extracted for the 17 AHA segments and defined cerebral territories, two visualization approaches were implemented and evaluated: (1) glyph-based representations and (2) surface-based representations. Both encodings target the comparison of regional tissue parameters between subgroups (G3) and the communication of intra-group variability (G4); they differ in how they balance spatial adjacency against overview, which motivates their comparative evaluation.

3.3.1. Color Scheme

To adapt the visualization to the conventions used by MRI imaging experts we chose the color legends suggested by the Color Recommendation Committee of the Quantitative MR Study Group of the International Society of Magnetic Resonance in Medicine (ISMRM) [FWC*25]. These color legends were recommended for 2D visualizations in the context of typically dark surroundings. For the usage with 3D visualizations and the avoidance of misperception through color mixes resulting from transparency, we set the background color to a gray value not present in the color maps (see Figure 5). Adopting community-standard relaxometry color maps [FWC*25] ensures that domain experts can interpret the mean-value channel using their established perceptual conventions, reducing cognitive load during cross-organ comparison (G1, G3). The neutral gray background was chosen because it lies outside all employed color maps, preventing transparency-induced color mixing from being misread as a data value (G4).

3.3.2. Glyph design

In this study, spherical glyphs were employed as geometric primitives, which were parametrically modified using a parameter mapping function (PMF) to encode both the mean and standard deviation for each segment and territory across the entire cohort. The mean parameter value was represented through color and size, whereas the standard deviation was encoded via anisotropic deformation (elongation) of the spherical glyph. Specifically, glyph size was determined using min–max normalization of the mean parameter values over the cohort. The elongation factor was derived by scaling the standard deviation relative to half of the global value

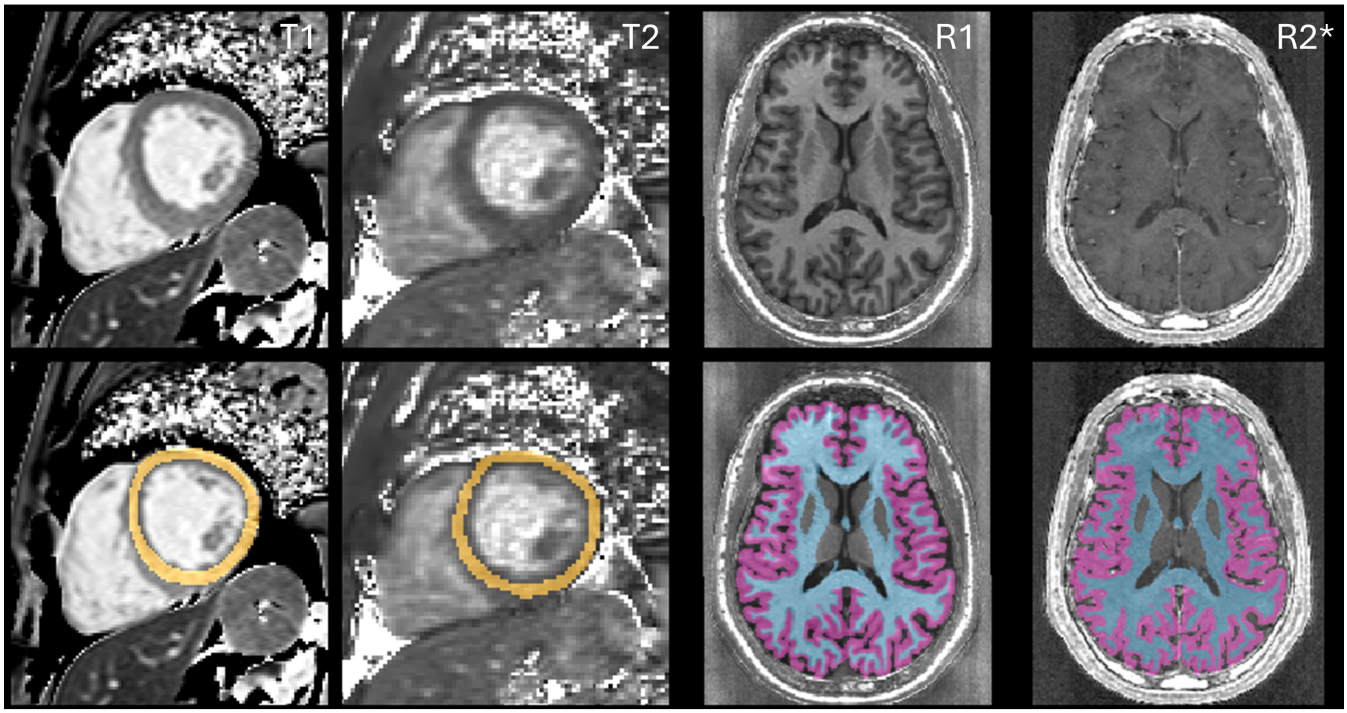

Figure 1: *Examples of T1 and T2 mapping of the heart; R1 and R2* mapping of the brain. Anatomical segmentations overlaid (bottom row): Left-ventricular myocardium (orange), gray (pink) and white (blue) matter.*

range:

$$\text{elongation} = s \cdot \left(1 + \frac{\sigma}{0.5 \cdot (\max_{\text{glob}} - \min_{\text{glob}})}\right)$$

where s denotes a predefined elongation scaling factor and σ represents the standard deviation of a parameter in one segment. This mapping follows established glyph-design guidelines for spatial multivariate medical data [ROP11]: the mean is assigned to size and color as separable, high-accuracy visual channels, whereas the standard deviation is mapped to glyph elongation, a distinct geometric channel that conveys variability (G4) without interfering with the mean. Decoupling the marks from the surface provides a simultaneous overview of all regions without view changes, supporting rapid cross-region comparison (G3).

3.3.3. Surface-Based Representation

In the second approach, statistical measures were directly encoded onto the anatomical surface models. The mean values were visualized using color mapping via predefined lookup tables (LUTs) [FWC*25], while the standard deviation was represented through transparency. Transparency (α) was inversely proportional to the normalized standard deviation:

$$\alpha = 1 - \frac{\sigma}{0.5 \cdot (\max_{\text{glob}} - \min_{\text{glob}})}$$

By mapping the mean directly onto contiguous anatomical regions, this encoding preserves spatial adjacency, which is exploited by the visual system to compare neighboring regions more reliably than spatially separated marks [AM22] (G1, G3). Variability is mapped to transparency as a secondary, lower-precision channel, so that highly variable regions recede visually and observed mean differences can be judged in the context of subgroup heterogeneity (G4).

3.3.4. Silhouette Enhancement

To improve the perceptual separation of subregions within the surface renderings, silhouette contours were added. This enhancement facilitated clearer delineation of anatomical structures and improved spatial interpretability. Silhouette contours were added because the semi-transparent surfaces and glyph overlays reduce figure–ground separation; explicit region boundaries restore the spatial delineation required to attribute a parameter value to the correct anatomical region (G1).

3.3.5. Visualization Scenarios

Based on the described techniques, two visualization scenarios were developed. Surface meshes representing the 17-segment AHA model [CWD*02] and the cerebral atlas [LHX*23] were employed. In the first scenario, semi-transparent surface meshes provided anatomical context, while glyphs encoded the statistical parameters. Glyphs were positioned at the centers of gravity of each AHA segment and cerebral territory and oriented toward the center of the respective model. In the second scenario, only the surface meshes were rendered, with mean and standard deviation encoded directly as described in the surface-based approach. This keeps each mark

A

L	R	
1	2	anterior cerebral artery
3	4	medial lenticulostriate
5	6	lateral lenticulostriate
7	8	frontal pars of middle cerebral artery
9	10	parietal pars of middle cerebral artery
11	12	temporal pars of middle cerebral artery
13	14	occipital pars of middle cerebral artery
15	16	insular pars of middle cerebral artery
17	18	temporal pars of posterior cerebral artery
19	20	occipital pars of posterior cerebral artery
21	22	posterior choroidal & thalamoperfurators
23	24	anterior choroidal & thalamoperfurators

B

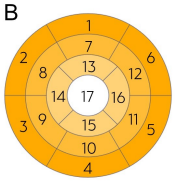

Basal	Mid-ventricular	Apical
1 anterior	7 anterior	13 anterior
2 anteroseptal	8 anteroseptal	14 septal
3 inferoseptal	9 inferoseptal	15 inferior
4 inferior	10 inferior	16 lateral
5 inferiolateral	11 inferiolateral	
6 anterolateral	12 anterolateral	17 apex

Figure 2: *A: Arterial territory atlas [LHX*23]. Numbering for left hemisphere only, right hemisphere is mirrored accordingly. B: 17-segment American Heart Association (AHA) model of the left ventricle [CWD*02].*

unambiguously associated with its region (G1), so that the two scenarios differ only in the encoding under comparison and can be evaluated fairly (G3).

3.3.6. Exploded View

Due to the close spatial proximity of gray and white matter regions within certain territories, glyph placement can lead to visual occlusion. To address this limitation, an exploded view was implemented, allowing spatial separation of these regions to improve visibility, interpretability and reliable readability (see Figure 3)(G1, G3).

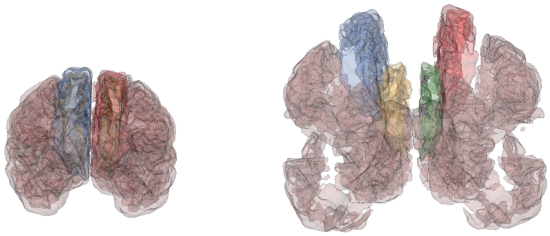

Figure 3: *Example of the explode view. Left: Original visualization of the cerebral surface mesh. Right: Exploded visualization, in which gray matter regions were moved from the center of gravity.*

3.4. Interaction

To support interactive exploration of the cohort, a PCP was used for subgroup selection. This visualization enables the simultaneous representation of multiple variables, including demographic characteristics, diagnoses, biomarkers, and risk factors, each mapped to an individual axis (Figure 4). By defining value ranges along one or more axes, subsets of cases can be interactively selected. The visualization frameworks described above are dynamically updated to reflect the selection, thus facilitating the exploration of multivariate relationships and patterns within the cohort.

3.5. User Interface

The user interface is organized into two main components. The upper panel comprises a PCP, which enables interactive subgroup selection based on user-defined variables. These variables include demographic characteristics, clinical diagnoses, and quantitative biomarkers, which can be flexibly configured as axes within the plot. The lower panel consists of a tab-based view that allows switching between different visualization modes. Each tab contains two synchronized 3D viewers that jointly depict cardiac and cerebral parameters. The left viewer presents the T1 mapping (heart) alongside the R1 mapping (brain), while the right viewer displays the T2 (heart) and R2* (brain) parameters. Both viewers have linked camera position and zoom level to ensure consistent spatial exploration across parameters and organs.

3.6. Implementation

The framework was implemented in MeVisLab [RBH*11]. The anatomical atlas surfaces are rendered using MeVisLab's integrated Winged-Edge-Mesh (WEM) library and its surface renderers, with color and transparency mapping applied via the described lookup tables. The spherical glyphs were realized as Open Inventor scenegraph primitives, parametrically modified according to the parameter mapping function in Section 3.3.2. The PCP was implemented in Python 3.13 using matplotlib [Hun07] and is coupled to the 3D viewers through MeVisLab's scripting interface, enabling the dynamic subgroup filtering described in Section 3.4.

4. Results

This section presents the application of the framework for the data of the BeLOVE cohort described in section 3.1.

All MRI datasets were processed with the pipeline described in section 3.2. The results were checked on a random basis, and the segmentations were found to be acceptable. Thus, the extracted features were added to the data frame for interactive visual exploration. We performed user tests with five users for two representative use cases to assess the applicability of the system using data from the BeLOVE study.

4.1. Use Case 1: Diagnosis-Related Differences

Diabetes and heart failure are both linked to diffuse myocardial tissue changes and cerebral microvascular alterations [SVM*26, GTYS25]. We therefore used the tool to explore whether regional

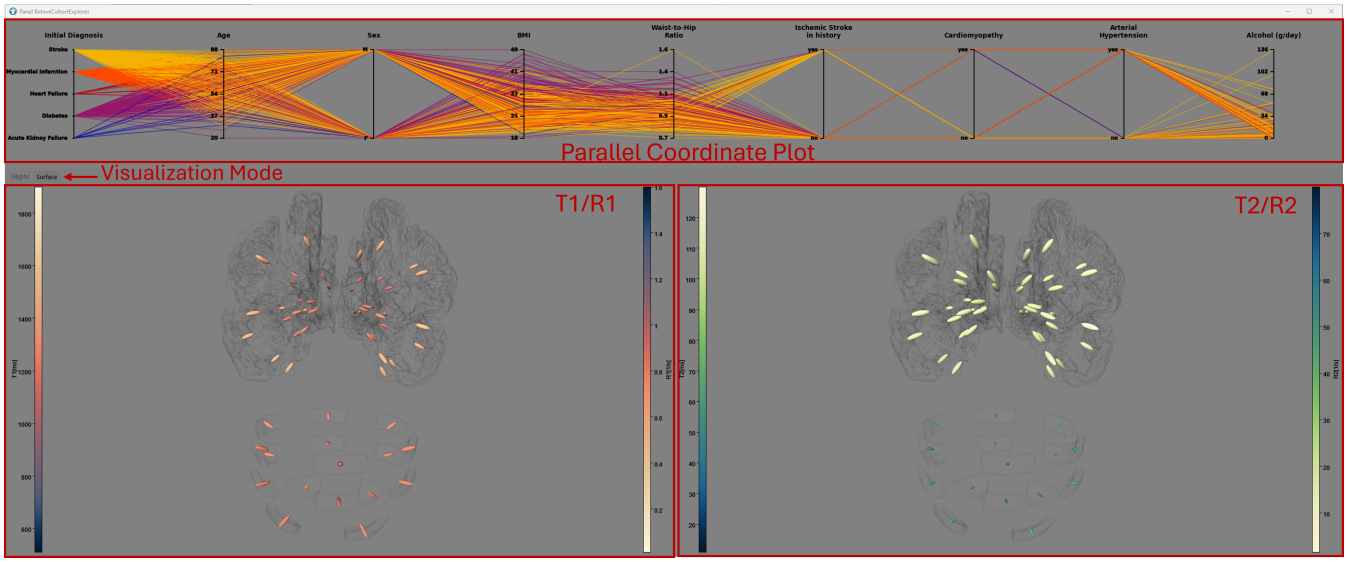

Figure 4: *User interface for the cohort exploration. The upper part shows the interactive parallel coordinate plot with colors representing the patients' diagnoses for the BeLOVE study. The tabs enable the selection of the visualization mode. The selected 3D visualizations of the atlas-related analysis of the MRI relaxometry data is shown in the lower part of the user interface.*

cardiac and cerebral parameter changes co-occur in these subgroups. Using the PCP, we selected patients with a history of heart failure (n = 9) and diabetes (n = 128). By interactively filtering the cohort using the PCP, corresponding changes in spatial parameter distributions across cardiac and cerebral regions could be observed, enabling the identification of potential patterns of organ cross-talk (figures 5 and 6). Such spatially corresponding cardiac–cerebral changes exemplify the heart–brain correspondences the tool is designed to reveal and can serve as starting points for confirmatory analysis.

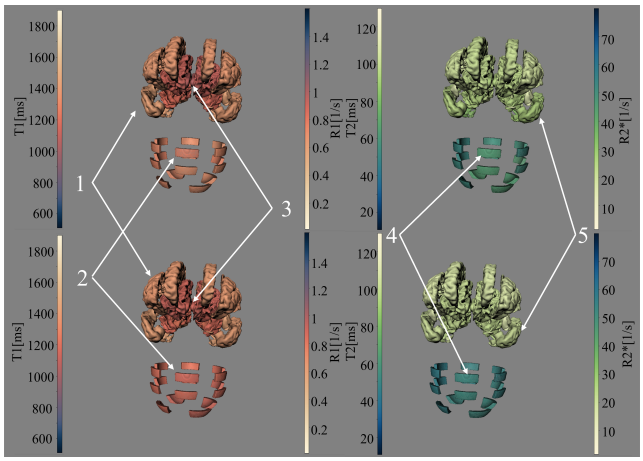

Figure 5: *Surface visualization for the subcohort selections in use case 1. Top: Visualization of mean T1, R1 (left) and T2, R2* (right) values for patients with heart failure. Bottom: Visualization of the same parameters for patients with diabetes. White arrows were added manually to highlight visible local differences.*

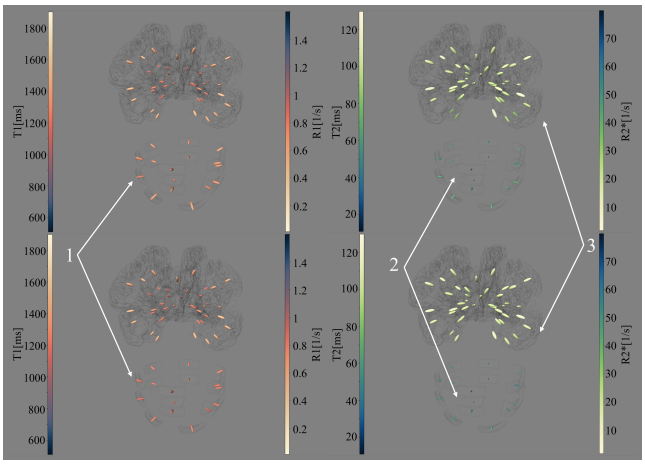

Figure 6: *Glyph visualization for the subcohort selections in use case 1. Top: Visualization of mean T1, R1 (left) and T2, R2* (right) values for patients with heart failure. Bottom: Visualization of the same parameters for patients with diabetes. White arrows were added manually to highlight visible local differences.*

4.2. Use Case 2: Obesity-Related Differences

Obesity is an established risk factor for both myocardial remodeling and cerebral microvascular and structural alterations, and is increasingly discussed as a shared driver along the heart–brain axis [SVM*26, GTYS25]. Using the PCP, we therefore contrasted a high-BMI subgroup (BMI 33–41 kg/m²) with a low-BMI subgroup (BMI 17–25 kg/m²) to explore whether obesity-associated tissue changes appear concurrently in cardiac and cerebral regions.

The visualization allowed exploration of variations in the parameters T1, T2 and R1, R2* between obese and non-obese individuals (figures 7 and 8).

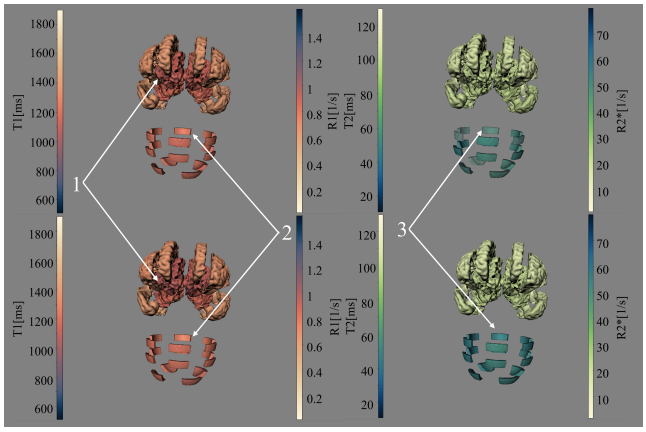

Figure 7: *Surface visualization for the subcohort selections in use case 2. Top: Visualization of mean T1, R1 (left) and T2, R2* (right) values for patients with a high BMI [33-41]. Bottom: Visualization of the same parameters for patients with a low BMI [17-25]. White arrows were added manually to highlight visible local differences.*

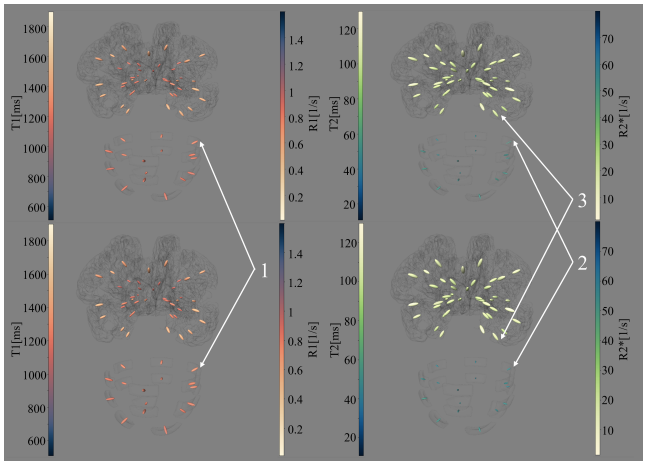

Figure 8: *Glyph visualization for the subcohort selections in use case 2. Top: Visualization of mean T1, R1 (left) and T2, R2* (right) values for patients with a high BMI [33-41]. Bottom: Visualization of the same parameters for patients with a low BMI [17-25]. White arrows added manually to point to regions with differences between patients with low and high BMI.*

4.3. User Study

The study assessed whether users could perceive sub-cohort differences and compared the interpretability of glyph vs. surface encodings; it was not designed to detect novel clinical correlations. The user study was designed as a formative assessment addressing two questions: can the coupled representations allow users to perceive regional differences between subgroups (G3), and which of the two spatial encodings better supports this perception. We did not aim to establish clinical validity of the findings, which requires a separate confirmatory study. Both visualization techniques and use cases were evaluated with five biomedical engineers (2 female). After a short introduction, each participant performed both use cases with both visualization modes and rated, on a 4-point scale, the clarity of perceived differences and of the spatial relationships. Each subgroup was selected individually in the PCP, and participants were able to repeatedly switch between the subgroup selections. We report the rating distributions below. Four users reported that the visual presentation of the interface made it easier to identify differences in the mean values and presented the spatial relationships more clearly. For use case 1, one user reported the changes to be *very clear*, three *rather clear*, one *less clear*, none unclear. For use case 2, two of the users reported the changes to be *very clear*, two *rather clear*, one *less clear*. One user reported that the spatial relationship was understood *very well*, four *well*, none *moderately* and none *poorly*.

4.4. Future Directions

The suggested processing pipeline could be successfully applied to all included datasets, and tissue parameters were automatically extracted from the maps. The general feedback from data exploration showed that the provided interaction and visualization concept enabled exploration of anatomy-related differences in tissue properties for subcohorts of patients of different diagnosis and BMI. User feedback indicated that changes in differences between neighboring anatomical regions could be perceived easier in surface visualizations than in glyph visualizations. This aligns with knowledge about perception theory, which indicates that differences between connected regions are easier to recognize than absolute differences between unconnected regions [AM22]. The glyph-based visualization enabled a complete overview of all regions without the need for view changes to explore the complete anatomical context. Thus, glyphs might be valuable for static visualizations, while the exploration of the easier interpretable surface visualization might benefit from user guidance through automatic view-of-interest calculation. The side-by-side visualization of the complementary data from the MRI relaxation times was difficult to interpret. To enable a joint perception, future approaches might combine the relaxation times via the orthogonal glyph dimensions or via color channels. A comparative mode could show two subcohorts side by side or map their difference directly onto the atlas, guiding the user to the regions of largest change automatically instead of relying on manual switching and inspection. A conceptual limitation is that summarizing each region by its mean and standard deviation collapses voxel-level spatial heterogeneity into scalar metrics. In this work these two moments were chosen deliberately to test the visual-encoding concept; the pipeline is designed to be extended toward richer local descriptors of tissue micro-structure, e.g. texture/radiomics features, which we plan to integrate and visualize using the same atlas-based framework.

5. Conclusions

We presented an image processing and exploration concept for inspection of local tissue properties of the brain and heart measured through MRI relaxation times in a study cohort. Anatomical atlases were used for the quantitative and visual analysis of spatially resolved differences between subgroups in the study cohort. The results indicate the usefulness of the approach, as well as future directions for a better integration of complementary information.

6. Acknowledgements

This work was supported by the Deutsche Forschungsgemeinschaft (DFG) through SPP-2177/515294457 and CRC-1470/B06, as well as the Deutsches Zentrum für Herz-Kreislauf-Forschung (DZHK) through MAP-HFpEF 81Z0100228. The system is built on the MeVisLab platform; the MeVisLab networks, glyph/surface modules, and the matplotlib-based PCP integration are available from the authors upon reasonable request.

References

[AM22] AGUILAR G., MAERTENS M.: Conjoint measurement of perceived transparency and perceived contrast in variegated checkerboards. *Journal of vision 22*, 2 (2022), 2. doi:10.1167/jov.22.2.2. 4, 7

[AOH*14] ANGELELLI P., OELTZE S., HAÁSZ J., ET AL.: Interactive visual analysis of heterogeneous cohort-study data. *IEEE Computer Graphics and Applications 34*, 5 (2014), 70–82. doi:10.1109/MCG.2014.40. 1, 2

[BLA*25] BEIZAEE F., LODYGENSKY G. A., ADAMSON C. L., ET AL.: Harmonizing flows: Leveraging normalizing flows for unsupervised and source-free MRI harmonization. *Medical Image Analysis 101* (4 2025). doi:10.1016/j.media.2025.103483. 2

[BSJ*14] BÖTTGER J., SCHURADE R., JAKOBSEN E., ET AL.: Connexel visualization: a software implementation of glyphs and edge-bundling for dense connectivity data using braingl. *Frontiers in Neuroscience Volume 8 - 2014* (2014). doi:10.3389/fnins.2014.00015. 2

[CNS*15] CHITIBOI T., NEUGEBAUER M., SCHNELL S., ET AL.: 3D superquadric glyphs for visualizing myocardial motion. In *Proceedings of the 2015 IEEE Scientific Visualization Conference (SciVis)* (USA, 2015), SCIVIS '15, IEEE Computer Society, p. 143–144. doi:10.1109/SciVis.2015.7429504. 2

[CWD*02] CERQUEIRA M. D., WEISSMAN N. J., DILSIZIAN V., ET AL.: Standardized myocardial segmentation and nomenclature for tomographic imaging of the heart. a statement for healthcare professionals from the Cardiac Imaging Committee of the Council on Clinical Cardiology of the American Heart Association. *Circulation 105*, 4 (2002), 539–542. doi:10.1161/hc0402.102975. 2, 3, 4, 5

[FWC*25] FUDERER M., WICHTMANN B., CRAMERI F., ET AL.: Color-map recommendation for MR relaxometry maps. *Magnetic Resonance in Medicine 93*, 2 (2025), 490–506. doi:https://doi.org/10.1002/mrm.30290. 3, 4

[GRF*24] GOFFI F., REALI P., FERRO A., ET AL.: Data-driven discovery of the central autonomic network: Dynamic integration of HRV and multivariate fMRI connectivity. In *2024 46th Annual International Conference of the IEEE Engineering in Medicine and Biology Society (EMBC)* (2024), pp. 1–5. doi:10.1109/EMBC53108.2024.10782925. 2

[GTYS25] GOH F. Q., TAN B. Y., YEO L. L., ET AL.: The heart-brain axis: Key concepts in neurocardiology. *Cardiology Discovery 5* (6 2025), 162–177. doi:10.1097/CD9.0000000000000156. 1, 5, 6

[HIT*22] HUELLEBRAND M., IVANTSITS M., TAUTZ L., ET AL.: A collaborative approach for the development and application of machine learning solutions for CMR-based cardiac disease classification. *Frontiers in Cardiovascular Medicine 9* (2022). doi:10.3389/fcvm.2022.829512. 2

[Hun07] HUNTER J. D.: Matplotlib: A 2d graphics environment. *Computing in Science and Engg. 9*, 3 (May 2007), 90–95. URL: https://doi.org/10.1109/MCSE.2007.55, doi:10.1109/MCSE.2007.55. 5

[IJK*21] ISENSEE F., JAEGER P. F., KOHL S. A. A., ET AL.: nnU-Net: a self-configuring method for deep learning-based biomedical image segmentation. *Nature Methods 18* (2 2021), 203–211. doi:10.1038/s41592-020-01008-z. 3

[JBF*20] JÖNSSON D., BERGSTRÖM A., FORSELL C., ET AL.: VisualNeuro: A hypothesis formation and reasoning application for multivariate brain cohort study data. *Computer Graphics Forum 39* (9 2020), 392–407. doi:10.1111/cgf.14045. 2

[KH13] KEHRER J., HAUSER H.: Visualization and visual analysis of multifaceted scientific data: A survey. *IEEE Transactions on Visualization and Computer Graphics 19* (2013), 495–513. doi:10.1109/TVCG.2012.110. 1, 2, 3

[LHX*23] LIU C. F., HSU J., XU X., ET AL.: Digital 3D brain MRI arterial territories atlas. *Scientific Data 10* (12 2023). doi:10.1038/s41597-022-01923-0. 2, 3, 4, 5

[LSW*26] LAUBE A. P., STEHNING C., WEBER J. E., ET AL.: Unsupervised image harmonization of multi-parametric maps of the brain [abstract 03790]. In *Proceedings of the ISMRM & ISMRT Annual Meeting & Exhibition 2026* (Cape Town, South Africa, May 2026). 2

[MBPA*25] MULTI CONSORTIUM, BOQUET-PUJADAS A., ANAGNOSTAKIS F., ET AL.: Brain-heart-eye axis revealed by multi-organ imaging genetics and proteomics. *Nat Biomed Eng* (2025), epub. doi:10.1038/s41551-025-01506-5. 2

[MHBS20] MÖRTH E., HALDORSEN I. S., BRUCKNER S., ET AL.: ParaGlyder: Probe-driven interactive visual analysis for multiparametric medical imaging data. In *Lecture Notes in Computer Science (including subseries Lecture Notes in Artificial Intelligence and Lecture Notes in Bioinformatics)* (2020), vol. 12221 LNCS, Springer Science and Business Media Deutschland GmbH, pp. 351–363. doi:10.1007/978-3-030-61864-3_29. 2

[MMD12] MANDAL P. K., MAHAJAN R., DINOV I. D.: Structural brain atlases: Design, rationale, and applications in normal and pathological cohorts. *Journal of Alzheimer's Disease 31* (2012). doi:10.3233/JAD-2012-120412. 2

[MNB*23] MEUSCHKE M., NIEMANN U., BEHRENDT B., ET AL.: GUCCI - Guided Cardiac Cohort Investigation of Blood Flow Data. *IEEE Transactions on Visualization and Computer Graphics 29*, 3 (2023), 1876–1892. doi:10.1109/TVCG.2021.3134083. 2

[MWP*07] MARCUS D. S., WANG T. H., PARKER J., ET AL.: Open access series of imaging studies (OASIS): Cross-sectional MRI data in young, middle aged, nondemented, and demented older adults. *Journal of Cognitive Neuroscience 19*, 9 (09 2007), 1498–1507. doi:10.1162/jocn.2007.19.9.1498. 3

[RBH*11] RITTER F., BOSKAMP T., HOMEYER A., ET AL.: Medical image analysis. *IEEE Pulse 2*, 6 (2011), 60–70. doi:10.1109/MPUL.2011.942929. 5

[ROP11] ROPINSKI T., OELTZE S., PREIM B.: Survey of glyph-based visualization techniques for spatial multivariate medical data. *Computers & Graphics 35*, 2 (2011), 392–401. doi:10.1016/j.cag.2011.01.011. 2, 4

[SMB*10] STEENWIJK M. D., MILLES J., BUCHEM M., ET AL.: Integrated visual analysis for heterogeneous datasets in cohort studies. In *IEEE VisWeek workshop on visual analytics in health care* (2010), vol. 3. 1, 2

[SVM*26] SCHEITZ J., VILLRINGER A., MIKAIL N., ET AL.: Bidirectional brain-heart interactions in health and disease. *Nat Rev Neurol. 22*, 4 (2026), 209–2025. doi:10.1038/s41582-025-01180-w. 1, 5, 6

[WAB*23] WEBER J. E., AHMADI M., BOLDT L. H., ET AL.: Protocol of the Berlin Long-Term Observation of Vascular Events (BeLOVE): A prospective cohort study with deep phenotyping and long-term follow up of cardiovascular high-risk patients. *BMJ Open 13* (10 2023). doi:10.1136/bmjopen-2023-076415. 1, 3

[WHL*20] WENTZEL A., HANULA P., LUCIANI T., ET AL.: Cohort-based t-ssim visual computing for radiation therapy prediction and exploration. *IEEE Transactions on Visualization and Computer Graphics 26*, 1 (2020), 949–959. doi:10.1109/TVCG.2019.2934546. 2, 3

[XCL*25] XU X., CAO Y., LIN G., ET AL.: Heart rate variability biofeedback alleviates subthreshold depression by reconstructing the brain-heart axis via habenular network functional connectivity modulation. *CNS Neurosci Ther 12* (2025), e70692. doi:10.1002/cns.70692. 2

[YSZG26] YANG Q., SHOMAL-ZADEH F., GHOLIPOUR A.: Harmonization in magnetic resonance imaging: A survey of acquisition, image-level, and feature-level methods. *Medical Image Analysis 111* (6 2026), 104066. doi:10.1016/j.media.2026.104066. 2

[ZDL*21] ZUO L., DEWEY B. E., LIU Y., ET AL.: Unsupervised MR, harmonization by learning disentangled representations using information bottleneck theory. *NeuroImage 243* (11 2021). doi:10.1016/j.neuroimage.2021.118569. 2

[ZLX*23] ZUO L., LIU Y., XUE Y., ET AL.: HACA3: A unified approach for multi-site MR image harmonization. *Computerized Medical Imaging and Graphics 109* (10 2023). doi:10.1016/j.compmedimag.2023.102285. 2